



cambridge.org/mrf

Nasrin Nasr Esfahani<sup>1</sup> , Dmytro M. Vavriv<sup>2</sup> and Klaus Schünemann<sup>1</sup>

<sup>1</sup>Hamburg University of Technology (TUHH), Am Schwarzenberg-Campus 1, 21073 Hamburg, Germany and  
<sup>2</sup>Institute of Radio Astronomy of the National Academy of Sciences of Ukraine (IRA NASU), 4, Mystetstv St., Kharkiv, 61002, Ukraine

## Research Paper

**Cite this article:** Nasr Esfahani N, Vavriv DM, Schünemann K (2023). A new class of spatial harmonic magnetrons with potentials for CW and sub-THz operation. *International Journal of Microwave and Wireless Technologies* **15**, 1308–1318. <https://doi.org/10.1017/S1759078723000065>

Received: 6 September 2022  
Revised: 23 January 2023  
Accepted: 24 January 2023

### Keywords:

Magnetron; meta-material; microwave tubes; sub-THz CW signal generators

### Author for correspondence:

Nasrin Nasr Esfahani,  
E-mail: [Nasrin.Esfahani@ieee.org](mailto:Nasrin.Esfahani@ieee.org)

### Abstract

A strictly physically based design theory of a new class of Spatial Harmonic Magnetrons (SHM) is thoroughly derived which leads to analytically evaluable expressions. Thus two advantages are obtained: (1) The design parameters appear grouped into two separate categories – one just containing geometrical and material parameters, the other one exclusively containing beam current-related ones, which are in product-form determining performance. The influence of each parameter can thus easily be discovered and investigated. (2) Numerical efforts for any new design will be reduced by at least one order of magnitude. Subsequently and based on feature (1) it is derived that loading the anode structure by a suitably selected meta-material will increase output power and efficiency, will pave the way to CW operation, and can extend oscillation frequency well into the sub-THz range. Finally, it is shown that the Rising Sun Magnetron is a first step toward a meta-material loaded SHM offering the same but quantitatively reduced features and less stringent requirements to fabrication technology.

## Vacuum electron devices and meta-materials

Veselago in his 1968 paper [1] predicted the reversal of conventional Cerenkov radiation in left-handed (LH) media. Since the introduction of the unit cells of an LH medium [2–4], reversed Cerenkov radiation (RCR) resulting from particle motion in such a medium attracted a lot of interest (for example see [5–12]), and in fact became the first research topic in the field of interaction of electron beams with meta-material. A backward radiation (backward with respect to the direction of motion of charged particles) from a transmission line based meta-material presented in [5] in 2002 was the first indirect experimental observation of RCR. Then in the next seven years, in a series of papers [6–9] by Kong and his team various aspects of these phenomena in meta-material have been extensively examined. In [6, 7], Cerenkov radiation in both isotropic and anisotropic LH media has been treated analytically. In [6], the effect of losses and dispersion has been thoroughly examined by considering a Drude-type permeability and permittivity, and it has been shown that in such a dispersive lossy medium both forward radiation (corresponding to conventional Cerenkov radiation) and backward radiation (corresponding to RCR) may exist. It has also been shown that the losses can affect the radiation angle. The realization of an appropriate 2D-DNG medium for experimental observation and verification of these phenomena has been presented in [8, 9].

The intrinsic relation between Cerenkov radiation and the fundamentals of operation of several classes of vacuum electronic devices (VEDs), including TWTs and BWOs, triggered another topic of research in the field of interaction of electron beams with meta-material (MTM), namely the application of meta-material in VEDs. This field of research which is less explored than RCR in meta-material, can be divided into three categories. The first category encompasses studies devoted to an investigation of instabilities which result from electron beams passing through meta-material slabs, and the effect of meta-material loading on the dispersion relation of VEDs. The second category deals with the implementation of meta-material as an effective medium in the slow wave structure (SWS) of VEDs. Advances in these two research categories paved the way for the third category of research, namely VEDs based on real meta-material unit-cells.

This paper can be associated with all these fields. It consists of two different parts: Its first, purely theoretical part deals with investigating an MTM loaded Spatial Harmonic Magnetron (SHM). It can be considered as an example of the first and the second category as defined above. We will hence briefly describe here the state-of-the-art of these two research categories. The second part of the present paper is a physical discussion of the consequences following from theory of the first part. From its nature, it belongs to the third category. Some results have already been sketched in a conference contribution [13] which deals with unit-cell based MTM loaded SHMs including realization and Particle-In-Cell (PIC) simulation.

© The Author(s), 2023. Published by Cambridge University Press in association with the European Microwave Association



The focus of the present discussion will be on the potentials of SHMs with MTM loading to offer stable operation at very low cathode current density. If this mode can be achieved with acceptable margins for output power and efficiency, CW operation will be possible. In this context, the Rising Sun Magnetron (RSM) will be investigated.

Examples of the first category of research can be found in [14–16]. In [14], it has been shown that the instabilities resulting from two electron beams passing through a hypothetical isotropic LH medium originate from RCR and that these instabilities can result in the self-modulation of the beam and radiation of electromagnetic waves, the phenomenon which is in fact quite similar to the process occurring in BWOs. The analysis of [14] is limited to the observation of these instabilities and does not include the implementation of these instabilities in a BWO. In [15], the hypothetical isotropic LH medium of [14] is replaced by two CSRR loaded parallel plates supporting a negative refractive index (NRI) TM mode. The interaction of this NRI TM mode with an electron beam passing through the parallel plates has been examined by modeling the electron beam by a dispersive permittivity and then extracting the dispersion relation of the structure. A similar approach has been implemented in [16] in order to model the interaction of an electron beam with a coaxial NRI transmission line based on meta-material. Implementing the proposed NRI structure in both a BWO or a TWT and investigating output power and efficiency of the structure in the presence of an electron beam have, however, not been treated in [15, 16].

Examples of the second category of research can be found in [17, 18]. In [17], which is among the first publications in the field of meta-material based VEDs, wave amplification in a DNG loaded folded waveguide traveling wave tube (FWTWT) has been examined using Madey’s theorem [19]. Analytical calculations confirm the possibility of wave amplification in such a structure, however, a comparison between this structure and its conventional counterpart in terms of important factors like e.g. gain has not been presented. In [18], an ENG loaded FWTWT has been examined. It has been shown that, at the cost of a reduced bandwidth, an ENG loading can considerably enhance the interaction impedance. PIC simulations confirm the superiority of the ENG loaded FWTWT to its conventional counterpart. It should be mentioned that in these simulations, the ENG medium is of Drude type and the effect of losses is neglected. In [20] as well as in [21], we have briefly reported that loading the SWS of a conventional SHM with an ENZ layer can improve the performance of these devices in terms of output power and efficiency.

The main purpose of this paper is presenting the detailed analysis that led us to the conclusion that ENZ loading of SHMs can provide the above mentioned advantages. In contrast to the classical magnetron, the operation conditions (operation mode, chosen harmonic, DC voltage, and magnetic field strength) in SHMs are selected in a way that the operation frequency of these sources can be easily extended into the mm-wave band, and even recently also into the sub-THz range [22–24]. With this goal in mind, in [20, 21], and also in this report, we have investigated this specific class of magnetrons. Several results have already been published in our paper [25] which is an extension of the conference paper [13], however, because of limited space, just gross results without any detailed derivation have been summarized and partially also discussed. There are two reasons for justifying the present publication: (1) Just by a detailed mathematical derivation, the decisive ideas and approximations can be made obvious which have led to an almost unique design theory implying surprising results, and

which ask for an extension to other VEDs. And (2), theory and conclusions have – for the first time – been extended to encompass the RSM. This technologically less ambitious alternative to the SHM with meta-material loading is thoroughly investigated and compared to the latter. Hence we do propose to study the present report in close relation to paper [25].

The paper is organized as follows: In its second section, the so-called “cold” analysis of a SHM loaded with a generally anisotropic medium is presented. The purpose of the “cold” analysis in which the effect of an electron beam is neglected, is calculating the resonant frequencies (i.e. the possible operation modes) and the amplitude and velocity of different Floquet harmonics of its SWS. The third section presents the so-called “hot” analysis (an analysis in the presence of the electron beam) of this novel SHM. This analysis shows the effect of employing ENZ layers in the SWS on both output power and efficiency of SHMs. The fourth and fifth sections deal with a thorough discussion of stability and a design example based on the effective medium approach. This study provides the guidelines for the unit-cell based realization of ENZ-loaded SHMs which had been presented in [13]. Finally, it will be pointed out in the sixth section that the RSM in principle also contains an inherent feature of an ENZ-loaded SHM or – generalized – of an SHM with meta-material loading: stable operation at extremely low current but still with high output power and efficiency. Hence CW operation should be possible at almost arbitrarily high frequency which is just limited by technological, but not by electro-magnetic requirements. Finally, a brief conclusion with an outlook will be presented.

“Cold” analysis of the meta-material loaded SHM

The SWS under consideration (Fig. 1(a)) consists of a cathode (radius  $r_c$ ) and an anode (radius  $r_a$ ) with  $N$  rectangular-type side resonators filled with an anisotropic medium with the following constitutive parameters:

$$\epsilon_s = \epsilon_0 \begin{bmatrix} \epsilon_x & 0 & 0 \\ 0 & \epsilon_y & 0 \\ 0 & 0 & \epsilon_z \end{bmatrix}, \quad \mu_s = \mu_0 \begin{bmatrix} \mu_x & 0 & 0 \\ 0 & \mu_y & 0 \\ 0 & 0 & \mu_z \end{bmatrix}. \quad (1)$$

The SWS height is  $h$ , and the resonator width and depth are  $d$  and  $l$ , respectively. The resonator opening angle is  $2\theta$ .

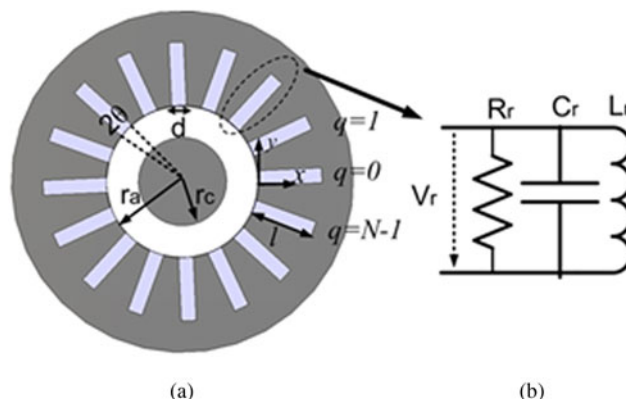


Fig. 1. (a) SWS structure of a SHM with side resonators filled with layers of an anisotropic medium and (b) equivalent circuit of the side resonators.

**Field components in the side resonators**

Important magnetron modes are TE modes without axial variation of the field. Due to the small width of the side resonators, the field variation in  $y$ -direction is also neglected in these resonators. The scalar and vector wave equations for these TE modes read:

$$\frac{\partial^2 H_z^{qC}}{\partial x^2} + k_x^2 H_z^{qC} = 0; \quad k_x^2 = k_0^2 \epsilon_y \mu_z, \quad (2)$$

$$E_y^{qC} = \frac{j\omega\mu_0}{k_0^2 \epsilon_y} \frac{\partial H_z^{qC}}{\partial x}, \quad H_x^{qC} = H_y^{qC} = E_z^{qC} = E_x^{qC} = 0, \quad (3)$$

where superscript  $q$  denotes the number that is devoted to each side resonator (see Fig. 1) and the superscript  $C$  shows that the fields are related to the cold analysis. The field components in each side resonator differ from those in the adjacent side resonator only by a constant phase difference which is equal to  $2\pi n/N$ , where  $n$  is an integer in between 0 and  $N/2$ . The operational mode of the magnetron is represented by either this phase difference or by  $n$ . Classical magnetrons operate at the  $\pi$ -mode (or the  $n = N/2$  mode) while SHMs usually operate at the  $\pi/2$ -mode (or the  $n = N/4$  mode) or at one of its neighboring modes. As can be expected, among the different elements of  $\epsilon_s$  and  $\mu_s$ , only  $\epsilon_y$  and  $\mu_z$  appear in the wave equations. Therefore we will assume that  $\epsilon_x = \epsilon_z = \mu_x = \mu_y = 1$ . Considering (2), (3), and the boundary conditions, the field components are determined by using (4.a) and (4.b) for the cases where  $\epsilon_y \mu_z > 0$  (i.e. DNG, DPS, ENZ ( $\epsilon_y \rightarrow 0^+$ ) and MNZ ( $\mu_z \rightarrow 0^+$ ) layers) and by using (5.a) and (5.b) for the cases where  $\epsilon_y \mu_z < 0$  (i.e. ENG, MNG, ENZ ( $\epsilon_y \rightarrow 0^-$ ) and MNZ ( $\mu_z \rightarrow 0^-$ ) layers):

$$H_z^{qC}(x, t) = jC e^{j(\omega t - (2\pi n/N)q)} \frac{\cos(k_x(l-x))}{\sin(k_x l)}, \quad (4.a)$$

$$E_\varphi^{qC}(x, t) = \eta_0 \eta_r C e^{j(\omega t - (2\pi n/N)q)} \frac{\sin(k_x(l-x))}{\sin(k_x l)}, \quad (4.b)$$

$$H_z^{qC}(x, t) = -jC e^{j(\omega t - (2\pi n/N)q)} \frac{\cosh(|k_x|(l-x))}{\sinh(|k_x|l)}, \quad (5.a)$$

$$E_\varphi^{qC}(x, t) = \eta_0 |\eta_r| C e^{j(\omega t - (2\pi n/N)q)} \frac{\sinh(|k_x|(l-x))}{\sinh(|k_x|l)}, \quad (5.b)$$

where  $\eta_0$  is the free space impedance and  $(\eta_r = \sqrt{\mu_z/\epsilon_y})$ .

In (4.b) and (5.b),  $\eta_0 |\eta_r| C$  is the amplitude of the electric field at the aperture of the side resonators. Here, similar to the approach used in some of the full wave simulators,  $C$  is determined in a way that the stored energy in that specific mode ( $U$ ) be equal to  $1J$ , i.e.:

$$U^C = \frac{1}{2} F C^2 = 1 \quad (6)$$

where  $F$  is the form factor of the SWS which is formulated in terms of the equivalent circuit parameters of the SWS.

**Field components in the interaction space**

The solution of the wave equation in the interaction space is a linear combination of Floquet harmonics (also called space harmonics) [26]:

$$\begin{aligned} H_z^{ic}(\rho, \varphi, t) &= \sum_{m=-\infty}^{\infty} H_{z_{m,n}}^{ic}(\rho, \varphi, t) \\ &= -jC \sum_{m=-\infty}^{\infty} A_m \frac{Z_{\gamma_m}(k\rho)}{Z'_{\gamma_m}(kr_a)} e^{j(\omega_n t - \gamma_m \varphi)}, \end{aligned} \quad (7.a)$$

$$\begin{aligned} E_\rho^{ic}(\rho, \varphi, t) &= \sum_{m=-\infty}^{\infty} E_{\rho_{m,n}}^{ic}(\rho, \varphi, t) \\ &= \frac{j\eta_0 C}{k\rho} \sum_{m=-\infty}^{\infty} A_m \gamma_m \frac{Z_{\gamma_m}(k\rho)}{Z'_{\gamma_m}(kr_a)} e^{j(\omega_n t - \gamma_m \varphi)}, \end{aligned} \quad (7.b)$$

$$\begin{aligned} E_\varphi^{ic}(\rho, \varphi, t) &= \sum_{m=-\infty}^{\infty} E_{\varphi_{m,n}}^{ic}(\rho, \varphi, t) \\ &= C \eta_0 \sum_{m=-\infty}^{\infty} A_m \frac{Z'_{\gamma_m}(k\rho)}{Z'_{\gamma_m}(kr_a)} e^{j(\omega_n t - \gamma_m \varphi)}, \end{aligned} \quad (7.c)$$

where the superscript  $iC$  refers to the fact that the fields are the interaction space fields resulting from cold analysis. In the rest of the equations of this report, subscripts  $m$  and  $n$  refer to the  $m$ th space harmonic and to mode number  $n$ , respectively, and  $Z_{\gamma_m}(k\rho)$  and  $Z'_{\gamma_m}(k\rho)$  are:

$$\begin{aligned} Z_{\gamma_m}(k\rho) &= J_{\gamma_m}(k\rho) - \frac{J'_{\gamma_m}(kr_c)}{Y'_{\gamma_m}(kr_c)} Y_{\gamma_m}(k\rho), \quad k = \omega_n \sqrt{\mu_0 \epsilon_0}, \\ Z'_{\gamma_m}(k\rho) &= J'_{\gamma_m}(k\rho) - \frac{J'_{\gamma_m}(kr_c)}{Y'_{\gamma_m}(kr_c)} Y'_{\gamma_m}(k\rho). \end{aligned} \quad (8)$$

$J, J',$  and  $Y, Y'$  are Bessel functions and their derivatives. As can be seen from (7.a) to (7.c), each space harmonic is characterized by a specific amplitude ( $A_m$ ) and a specific phase velocity around the interaction space ( $\dot{\varphi} = \omega/\gamma_m$ ). The boundary condition for the electric field at the interface between the side resonators and the interaction space determines these amplitudes and also the propagation constant  $\gamma_m$ :

$$\begin{aligned} A_m &= \sqrt{\left| \frac{\mu_z}{\epsilon_y} \right|} \frac{N\theta \sin \gamma_m \theta}{\pi \gamma_m \theta}, \\ \gamma_m &= mN + n \quad m = \dots, -1, 0, 1, \dots; \quad n = 0, 1, \dots, \frac{N}{2}. \end{aligned} \quad (9)$$

Since we have neglected the higher order modes in the side resonators, the boundary condition for the magnetic field can only approximately be satisfied:

$$\int_{(2\pi q/N)-\theta}^{(2\pi q/N)+\theta} H_z^I(r_a, \varphi) r_a d\varphi = \int_{d/2}^{-d/2} H_z^q(r_a) dy. \quad (10)$$

Equation (10) results in the following expression which determines the resonant frequencies of different modes:

$$\sum_{m=-\infty}^{\infty} \frac{N\theta}{\pi} \left( \frac{\sin \gamma_m \theta}{\gamma_m \theta} \right)^2 \frac{Z_{\gamma_m}(kr_a)}{Z'_{\gamma_m}(kr_a)} = \begin{cases} \sqrt{(\epsilon_y/\mu_z) \cot(k_x l)} & \text{if } k_x^2 > 0 \\ \sqrt{|(\epsilon_y/\mu_z)| \coth(|k_x l|)} & \text{if } k_x^2 < 0 \end{cases} \quad (11)$$

In the next section, an approximate expression for the output power in SHMs in terms of the EM fields calculated in this section will be presented.

### Formulation of the output power for the meta-material loaded SHM

Since an effective interaction mainly occurs between the rotating electrons and the space harmonic which is in synchronism with these electrons, only this harmonic of the field will be considered in the beam wave interaction equations. It should be mentioned that the synchronous harmonic in SHMs is the first backward harmonic ( $m = -1$ ), while in classical magnetrons the fundamental harmonic ( $m = 0$ ) is the synchronous one. When a convection current of density  $\vec{J}_{C_{m,n}}$  flows in an electric field of  $\vec{E}_{m,n}^{ie}$  (superscript i.e. refers to the fact that the fields are the interaction space fields and they are resulted from the analysis which takes the presence of the electron beam into account) with the same frequency and spatial periodicity (i.e. the same  $m$  and  $n$ ), the complex power transferred from the electrons to the electric field will be:

$$P_c = P_e + jP_r = \frac{1}{2} \iiint \vec{J}_{C_{m,n}}(\rho, \varphi, t) \vec{E}_{m,n}^{ie*}(\rho, \varphi, t) \rho d\rho d\varphi dz, \quad (12)$$

where  $P_e$  means real power that is transferred to the field. It shall be called the electron power.  $P_r$  is the reactive power which flows back and forth between field and electrons and  $\vec{E}_{m,n}^{ie}$  and  $\vec{J}_{C_{m,n}}$  are:

$$\begin{aligned} \vec{E}_{m,n}^{ie}(\rho, \varphi, t) &= E_{\varphi_{m,n}}^{ie}(\rho, \varphi, t) \hat{a}_\varphi + E_{\rho_{m,n}}^{ie}(\rho, \varphi, t) \hat{a}_\rho \\ &= a(t) e^{j(\varphi_f(t) - \gamma_m \varphi)} (E_{\varphi_{m,n}}^{ic}(\rho, \varphi, t) \hat{a}_\varphi + E_{\rho_{m,n}}^{ic}(\rho, \varphi, t) \hat{a}_\rho), \end{aligned} \quad (13.a)$$

$$\begin{aligned} \vec{J}_{C_{m,n}}(\rho, \varphi, t) &= J_{c\varphi_{m,n}}(\rho, \varphi, t) \hat{a}_\varphi + J_{c\rho_{m,n}}(\rho, \varphi, t) \hat{a}_\rho \\ &= a(t) e^{j(\varphi_f(t) - \gamma_m \varphi)} (J'_{c\varphi_{m,n}}(\rho, \varphi, t) \hat{a}_\varphi + J'_{c\rho_{m,n}}(\rho, \varphi, t) \hat{a}_\rho). \end{aligned} \quad (13.b)$$

In (13.a) and (13.b),  $a(t)$ ,  $\varphi_f(t)$ ,  $\varphi_C(t)$ ,  $J_{c\varphi_{m,n}}(\varphi, \rho)$ ,  $J_{c\rho_{m,n}}(\varphi, \rho)$ , and  $J'_{c\varphi_{m,n}}(\varphi, \rho)$  and  $J'_{c\rho_{m,n}}(\varphi, \rho)$  are slowly varying functions of time, and  $E_{\varphi_{m,n}}^{ic}(\varphi, \rho)$  and  $E_{\rho_{m,n}}^{ic}(\varphi, \rho)$  are determined using (7.b) and (7.c). In a similar way, the field components of the side resonators in the presence of the electron beam can also be written in terms of the field components resulting from the cold analysis ((4) and (5)) as follows:

$$H_z^{qe}(x, t) = a(t) e^{j\varphi_f(t)} H_z^{qC}(x, t), \quad (14.a)$$

$$E_\varphi^{qe}(x, t) = a(t) e^{j\varphi_f(t)} E_\varphi^{qC}(x, t), \quad (14.b)$$

where superscript  $qe$  refers to the fact that the fields of the  $q$ th side resonator result from the analysis in the presence of the electron beam.

Considering the continuity equation for the convection current, we have:

$$\frac{\partial r J_{C_{\rho_{m,n}}}(r, \varphi, t)}{\partial r} + \frac{\partial J_{C_{\varphi_{m,n}}}(r, \varphi, t)}{\partial \varphi} = -r \frac{\partial \rho}{\partial t}. \quad (15)$$

Combining (7.b), (7.c), (13.a), (13.b), and (15) with (12) yields

$$\begin{aligned} P_c &= P_e + jP_r \\ &= \frac{A_{-1} Ca(t)}{2} \eta_0 X (\cos \Delta\varphi(t) + j \sin \Delta\varphi(t)), \end{aligned} \quad (16)$$

where  $\Delta\varphi(t)$  is the phase difference between the  $\varphi$ -directed electric field and the convection current, and

$$X = \int \left( \frac{\gamma_m^2 Z_{\gamma_m}(k\rho)}{k\rho Z'_{\gamma_m}(kr_a)} J_{\rho_{cm,n}}(\rho, \varphi, t) + \frac{Z'_{\gamma_m}(k\rho)}{Z'_{\gamma_m}(kr_a)} J_{\varphi_{cm,n}}(\rho, \varphi, t) \right) dv. \quad (17)$$

Considering the energy conservation equation, it can be concluded that [23]:

$$\frac{dU^e}{dt} = P_e - P_{loss} - P_{out}, \quad (18)$$

where  $dU^e/dt$  is the time rate of the potential energy variations,  $P_{loss}$  is the sum of the losses, and  $P_{out}$  means output power. Since  $P_{loss} + P_{out} = \omega_n U^e / Q_l$ , where  $Q_l$  is the loaded quality factor, relation (18) can be further simplified to read:

$$\frac{dU^e}{dt} = P_e - \frac{\omega U^e}{Q_l}. \quad (19)$$

On the other hand,  $P_r$  which appears as result of the phase difference between the electric field and the convection current, contributes to a frequency shift as follows:

$$\Delta\omega = \frac{d\psi}{dt} = \frac{-P_r}{2U}. \quad (20)$$

From (14), the amplitude of the voltage at the aperture of the side resonators in the presence of an electron beam is

$$V^e = \eta_0 \eta_r Ca(t) d, \quad (21)$$

where  $d$  means width of the side resonators (see Fig. 1(a)).

Considering (6) and (14),  $U^e$  reads

$$U^e = a^2(t) U^C = a^2(t). \quad (22)$$

Then combining (16) and (22) with (19) results in

$$2a(t) \frac{da(t)}{dt} = \frac{A_{-1} Ca(t) \eta_0 X \cos \Delta\varphi}{2} - \frac{\omega_n a^2(t)}{Q_l}. \quad (23)$$

The value of  $a(t)$  in the steady state condition ( $a$ ) can be calculated from:

$$a = \frac{A_{-1}X\eta_0Q_lC \cos \Delta\varphi}{2\omega_n}, \tag{24}$$

where  $\Delta\varphi$  is the steady state value of the phase difference between the  $\varphi$ - directed electric field and the convection current.

Considering the steady state condition ( $du/dt \rightarrow 0$ ) and using (16) and (24),  $P_e$  can be calculated from

$$P_e = \frac{(A_{-1}C\eta_0X \cos \Delta\varphi)^2 Q_l}{4\omega_n} = \frac{(A_{-1}C\eta_0X \cos \Delta\varphi)^2 Q_u Q_{ext}}{4\omega_n(Q_u + Q_{ext})}, \tag{25}$$

where  $Q_{ext}$  and  $Q_u$  are the external and unloaded quality factor, respectively.

For the non- $\pi$  operation modes, the stored energy and the losses in the interaction space are negligible in comparison to the stored energy and the losses in the side resonators [22]. Therefore the side resonators of the SHM  $\pi$  are modeled with parallel resonant circuits as is shown in Fig. 1(b). The stored energy ( $U$ ), losses ( $P_{loss}$ ), and the unloaded quality factor of the SWS of a SHM can be calculated using [22]:

$$U^e = \frac{N}{2\omega^2} \frac{V^{e2}}{L}, \tag{26}$$

$$P_{loss} = \frac{N}{2} \frac{V^{e2}}{R}, \tag{27}$$

$$Q_u = \frac{R}{L\omega_n}, \tag{28}$$

where  $L$  and  $R$  are the equivalent inductance and resistance, respectively, of the side resonators, and  $V^e$  is determined using (21).

By combining (26) with (22) and (21),  $C$  can be calculated yielding:

$$C^2 = \frac{2\omega_n^2}{N} L\eta_r^{-2}\eta_0^{-2}d^{-2}. \tag{29}$$

For the DPS, ENZ ( $\epsilon_y \rightarrow 0^+$ ) and MNZ ( $\mu_z \rightarrow 0^+$ ) layers for which  $\epsilon_y$  and  $\mu_z$  are slowly varying function of frequency, the equivalent inductance and resistance of the side resonators can be determined using (30) and (31):

$$L = \frac{V^{e2}}{\omega_n^2\mu_0\mu_z \int |H_z^{qe}|^2 dv} \tag{30}$$

$$R_r = \frac{V^{e2}}{\sqrt{(\omega_n\mu_0/2\sigma)} \int |H_z^{qe}|^2 ds} \tag{31}$$

where  $\sigma$  is the conductivity of metal and  $H_z^{qe}$  is the magnetic field in the side resonators which can be determined from (14.a) under steady state conditions.

It should be noted that for other types of meta-material which have been mentioned in the second section, the dispersion effects cannot be neglected, so that relations (30) and (31) cannot be used for calculating the equivalent  $L$  and  $R_r$ .

Evaluating the integrals in (30) and (31) yields:

$$L = \frac{2d\sin^2(k_x l \partial)}{\omega^2 \epsilon_\varphi \epsilon_0 H l (1 + (\sin(2k_x l)/2k_x l))}, \tag{32}$$

$$R_r = \frac{\mu_z \mu_0 / \epsilon_\varphi \epsilon_0 d^2 \sin^2(k_x l)}{\sqrt{(\omega_n \mu_0 / 2\sigma)} H l (1 + (\sin(2k_x l)/2k_x l) + (d/l))}. \tag{33}$$

From (28), (32), and (33),  $Q_u$  can be calculated:

$$Q_u = \frac{\omega \mu_z \mu_0 d (1 + (\sin(2kl)/2kl))}{2\sqrt{(\omega_n \mu_0 / 2\sigma)} (1 + (\sin(2kl)/2kl) + (d/l))}. \tag{34}$$

Now using (21), (24), (28), and (29),  $V^e$  can be simplified to

$$V^e = \frac{A_{-1}R_t}{N\eta_r d} X \cos \Delta\varphi, \tag{35}$$

where  $R_t$  is calculated from:

$$R_t = R \frac{Q_{ext}}{Q_{ext} + Q_u}. \tag{36}$$

Now combining (25) with (33), (29), and (28) results in:

$$P_e = \frac{N V^{e2}}{2R_t}. \tag{37}$$

Considering (36) and  $Q_{ext} \rightarrow \infty$ , the electron power for the unloaded case  $P_e^U$  can be calculated using:

$$P_e^U = \frac{N V^{eU2}}{2R_t}, \tag{38}$$

where  $V^{eU}$  is:

$$V^{eU} = \frac{A_{-1}X R}{\eta_r d N} \cos \Delta\varphi. \tag{39}$$

Relation (37) allows a very simple interpretation: the electron power in the magnetron is equal to the sum of the dissipated power in the side resonators with an equivalent resistance of  $R_t$ . Although to the best of our knowledge, a detailed extraction of (37) has not yet been presented in literature, its accuracy in the case of conventional magnetrons has been examined by numerical simulations [27].

Now considering (18) and (19) at the steady state condition, the output power can be calculated:

$$P_{out} = \left(1 - \frac{Q_l}{Q_u}\right) P_e, \tag{40}$$

where  $P_e$  is calculated using (37).

As is explained in the next section, the bunching process in magnetrons is governed by the synchronous harmonic of the

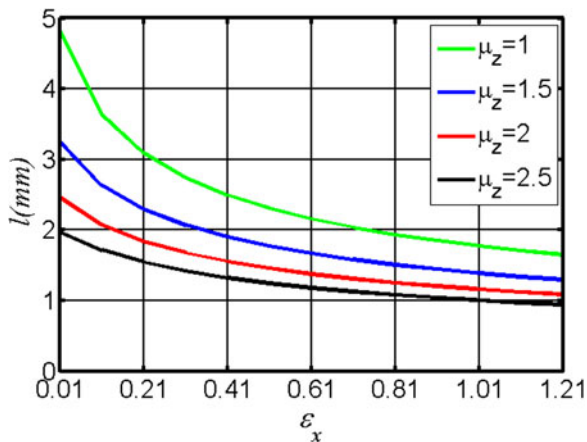


Fig. 2. Length of the side resonators for different values of  $\mu_z$  and  $\epsilon_y$ .

radially directed electric field ( $E_{\rho m,n}^{ie}(\rho, \varphi, t)$ ). Considering (7.b), (13.a), (21), and the fact that  $\gamma_m$  is a large value in SHMs, it can be concluded that this component is equal to:

$$E_{\rho m,n}^{ie}(\rho, \varphi, t) = \frac{A_{-1}}{\eta_r} V^e e^{j(\varphi_j(t) - \gamma_m \varphi)} \frac{1 - (r_c/\rho)^{2\gamma_m}}{1 + (r_c/\rho)^{2\gamma_m}} \quad (41)$$

From (41) and (39), it can be derived that the maximum amplitude of  $E_{m,n}^{ie}$  is proportional to the product of a term  $T_g$  that contains all geometrical and constitutive parameters related to the SHM, and a term  $T_j$  just related to the current flow in the interaction space, i.e.:

$$|E_{\rho m,n}^{ie}(\rho, \varphi, t)| \propto T_g T_j, \quad (42)$$

where  $T_g$  and  $T_j$  are defined by:

$$T_g = \frac{A_{-1}^2 R_t}{N \eta_r^2 d}, \quad T_j = X \cos \Delta\varphi. \quad (43)$$

This separation of dependencies is of prominent importance for practical SHM design.

### Bunching process and the relation between geometrical parameters and the current flow

We are in a position now to investigate in detail the dynamics of bunching and hence of power generation in a magnetron. To this end we regard an electron beam flowing through the interaction space, and specify the situation in an arbitrary cross-section. In this two-dimensional space, the electron beam appears as an ensemble of spokes due to the effect of bunching. The power generation procedure reflects itself in the relative positions of e.g. a single bunch of a clockwise rotating electron spoke-like beam with respect to the synchronous harmonic of the electric field, when the phase difference between the current and the electric field is equal to zero ( $\Delta\varphi = 0$ ) so that the magnetron generates its maximum output power. At this condition, the electrons at the right and left-hand side of the bunch are affected by equal but oppositely directed radial components of the synchronous harmonic of the electric field ( $+\alpha, -\alpha$ ) and by an equally directed DC field  $E_{DC}$ . Any electron that precedes the bunch due to an

excess in its velocity ( $v$ ) will be slowed down according to  $v = (E_{DC} - \alpha)/B$ , where  $B$  is the magnetic field. On the other hand, any electron that lags the bunch due to its smaller velocity will experience an increase in velocity according to  $v = (E_{DC} + \alpha)/B$ . The process of slowing down the fast electrons at the right edge of the bunch and accelerating the slow electrons at the left edge explains the formation of the electron bunch. As far as the average value  $\bar{E}$  of the electric field which is experienced by the electrons at the center of the bunch  $\bar{E}$  (for  $\Delta\varphi = 0$ , it is equal to  $E_{DC}$ ) is in appropriate proportion to the maximum variation of the electric field, which is affecting the electrons  $2\tilde{E}$  (for  $\Delta\varphi = 0$ , it is equal to  $2\alpha$ ), the electron bunch preserves its phase difference with the electric field. Now if we increase  $\tilde{E}$  (for example by increasing the geometrical term  $T_g$ ), the appropriate proportion between  $\bar{E}$  and  $\tilde{E}$  will not exist any longer. A magnetron responds to this situation by increasing  $\Delta\varphi$  which results in increasing  $\bar{E}$  to  $E_{DC} + (\alpha' + \beta'/2)$  (where  $\alpha'$  and  $\beta'$  are radially directed components of the synchronous harmonic of the electric field). On the other hand, if we decrease  $\tilde{E}$  (for example by decreasing the geometrical term  $T_g$ ), the magnetron restores the appropriate proportion between  $\bar{E}$  and  $\tilde{E}$  by decreasing  $\Delta\varphi$  which results in decreasing  $\bar{E}$  to  $\tilde{E} - (\alpha' + \beta')/2$  and effective bunching of the electrons.

Thus it is shown by an imaginary experiment that tuning the SHM for optimum output power, simultaneously means establishing stable operation. Another conclusion is that according to relations (42) and (43), any change in e.g. one of the geometrical (or current) parameters can be compensated by an appropriate change in one of the current (or geometrical) parameters. This result is of paramount importance for both magnetron design (namely optimization of the various parameters w.r.t. output power) and operation. While the former procedure is drastically simplified (by reducing the simulation work from weeks to days – or at least from days to hours, if useful initial values are at hand), the latter feature (i.e. the separation of geometrical from current parameters within the criterion of stable operation) shall open a completely new field for magnetron operation: It seems to be possible to reduce the minimum required cathode current density down to values which do not mean an appreciable thermal load for the tube. Hence even CW operation at up to THz frequencies should be possible for meta-material loaded SHMs, thus enabling completely new fields of applications: non-pulsed = CW systems for remote sensing (radars) and communications (micro-cell radio) etc.

### Design examples

The main purpose of this part is showing the positive effect of loading the side resonators of a magnetron with a large  $\sqrt{(\mu_z/\epsilon_y)}$ , i.e., either an ENZ medium or a medium with a large  $\mu_z$ . For this purpose we consider an  $n = 4$  (or  $\pi/2$ )-mode 35 GHz SHM with  $r_a = 2.25$  mm,  $r_c = 1.3$  mm,  $N = 16$ ,  $N\theta/\pi = 0.5$ . The length of the side resonators ( $l$ ) has been calculated using (11). Accuracy of this equation has been examined in [28] (Fig. 2)

Combining (37) with (39), and (43), we have:

$$P_e \propto (T_g T_j)^2 \quad (44)$$

Now the ratio of geometrical term  $T_g$  for a conventional magnetron versus a metamaterial loaded one  $T_g(\mu_z, \epsilon_y)/T_g(1,1)$  can be calculated using (43), (36), (34), (33), (9) for the magnetron

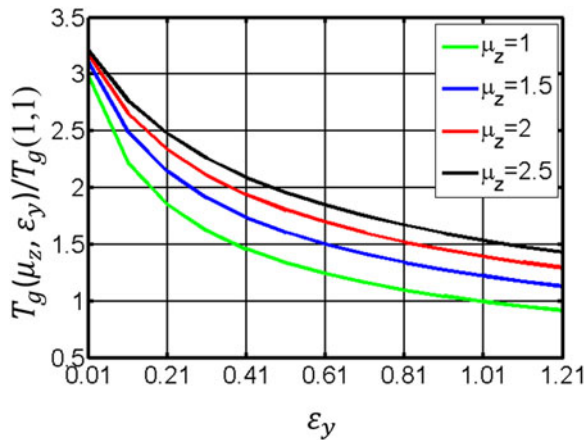


**Fig. 3.** Ratio of geometrical term for a conventional and a metamaterial loaded magnetron.

dimensions given in the beginning of this section and for different pairs of  $\mu_z$ ,  $\varepsilon_y$  as shown in Fig. 3.

As seen in this figure,  $T_g$  and as a result the  $P_e^U$  of an ENZ loaded SHM can be much larger than that of a conventional SHM. The positive effect of increasing  $\mu_z$  on the electron power for a tube with normal SWS can also be deduced from this figure.

Future investigations should hence try to explain the mechanism by which the “hot” term part and the “cold” term part of the electron power will affect each other. Such (possible) effect will probably establish an upper limit for  $P_e^U(\varepsilon_y, \mu_z)/P_e^U(1, 1)$ . To prepare for corresponding future investigations, the necessary formulas have been summarized in the Appendix.

For a complete design of a MTM-loaded SHM, the reader is referred to [25], the source of the present report. According to relation (42), the output power can be enhanced by increasing the factor  $T_g$  of the geometrical and constitutive parameters. This leads to loading the side resonators with an ENZ medium which in case of a SHM can e.g. be realized by unit cells from complementary square open loop resonators (CSOLRs). This is illustrated by a longitudinal section through a 42 GHz magnetron block depicted in Fig. 4. In total, 16 side resonators are formed by 8 vanes representing CSOLRs and another 8 solid vanes.

All details about design, calculations of resonant frequencies and effective permittivity and permeability, about the excellent validity of the effective medium approach, about mode competition and bandwidth broadening, and about fabrication are discussed in [25]. In the context of the present paper, a special discovery is of particular importance: Stable oscillations of this class of MTM loaded SHMs do even occur at especially low cathode current densities although output power and efficiency remain on high level. This feature seems to be a unique one. It cannot be achieved with the conventional SHM, because just the MTM loaded SHM offers a way to decrease (even drastically) cathode current and thus the factor  $T_j$  in (42), too. Following the discussion in Sec. IV about how to establish stable oscillations, such decrease must and can be compensated by an appropriate increase of factor  $T_g$ . This is an inherent feature of MTM loaded SHMs leading to powerful (and unique) consequences: Continuous wave (CW) operation should be possible at simultaneously interesting (competitive) margins for power and efficiency whereas any limitation in frequency is just imposed by technological but not by electro-magnetic requirements. Hence

## 42 GHz MTM-SHM

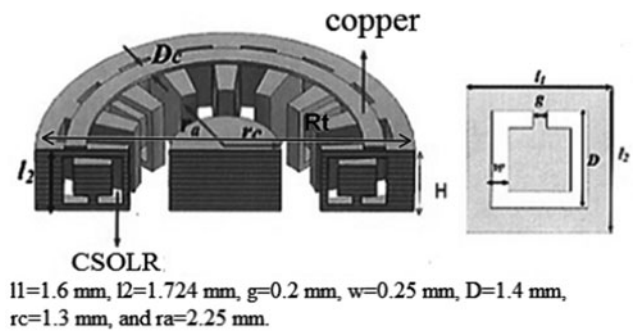


**Fig. 4.** Section through a MTM loaded 42 GHz SHM.

sub-THz CW sources with power and efficiency well above those of a BWO seem to be in reach. They had apparently the potentials to revolutionize many actual and important applications in various commercial, technical, and scientific fields.

Thus this new class of SHMs defines a new independent class of high frequency devices which could be called “MTM-SHMs”.

### The rising sun-structure alternative

The preceding discussions of MTM-SHM performance have shown that there do exist stable oscillation regimes at very small cathode current density so that even CW operation with still high output power should be possible. One should hence complete the 3 operation scenarios which have been defined and discussed by McDowell in [27, 29] and in the context of our SHM investigations in [28] by adding a fourth one. Then they read

- (1) Space charge limited operation: Primary emission with maximum current, mainly used for industrial heating applications.
- (2) Secondary emission dominated operation: Large current from cold cathode, very high pulsed power; alternatively, SHM mode for high frequencies.
- (3) Emission limited operation: Small current from a thermionic cathode, no secondary emission cathode, CW mode just at low frequencies.
- (4) Secondary emission limited operation: Very small current from cold cathode, potentials for CW mode at even very high frequencies.

The MTM-SHM is belonging to the fourth scenario. To realize this mode of operation, the geometrical factor in (42) or – in general words – a suitable design of the anode structure have been utilized to minimize beam current without affecting stability of oscillations at still high output power. Such a means is not offered by the conventional SHM in which there is an upper numerical limit for the synchronous spatial harmonic. (A rigorous analysis of its SWS yields a limit of  $<0.42$ .) Hence conventional SHMs can only be operated in high current, i.e. in pulsed mode. However, such limit does not exist in case of a RSM. Invoking the cathode emission model (see [29]) into Microwave Studio program package, it could be shown by simulations that again output power is proportional to the synchronous Floquet amplitude, but that there does not exist an upper limit for this amplitude. This is a first hint that small enough beam current values should be

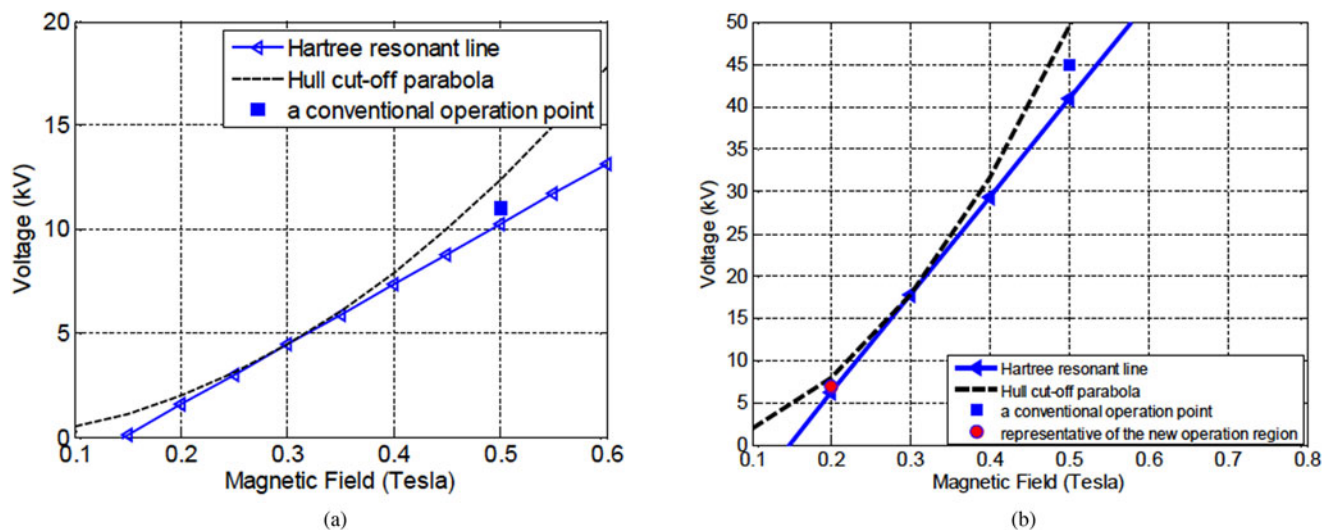


Fig. 5. Beam voltage versus magnetic field with boundary curves for a magnetron at 35 GHz for an (a) conventional SHM (left) and (b) RSM with enlarged anode (right).

achievable, and that thus CW operation might be in reach with a RSM, too.

The physical model of the MTM-SHM has explained bunching process and stability as result of a delicate balance between the radially directed components of both the electric DC and the AC field of the first backward harmonic, which must be established by “tuning” the geometrical and the current parameters in (42). Strongly decreasing cathode current in order to establish CW operation conditions, directly leads to MTM anode structures which can show high values for both geometrical parameter and output power. As “soft” alternative to such SWS – although its positive effect on output power seems to be less strong –, a rising-sun-like anode also offers the potential for low-current operation, but at reduced technological complexity. Compared to the MTM-SHM, the RSM presents a trade-off between high performance and severe fabrication problems. It is technologically less challenging.

Hence it is worth investigating theory and features of a RSM in depth inasmuch as it is an interesting alternative to the SHM. Up to now, it has just been shown that the RSM output power is larger than that of the SHM. However, analyzing the known experimental data augmented by simulations by applying the basic ideas which have been developed in the MTM-SHM model, one can detect several hints about more and interesting differences to SHM performance. This is mainly the feature that there seems to exist kind of a geometrical factor which can be increased without deteriorating stability of oscillations. Instead one observes maximizing of the synchronous and minimizing of the fundamental spatial harmonic at reduced beam current.

The analytical description of the RSM closely follows the scheme of sections “Cold” analysis of the meta-material loaded SHM’ and ‘Formulation of the output power for the meta-material loaded SHM’. The anode block is modeled by an equivalent network in which the side resonators are represented by two RLC circuits due to that a RSM anode consists of two sets of side resonators of different radial extension. Their parameters are determined from both the energy stored and the Ohmic losses. This means solving Maxwell’s equations for the EM field in the side resonators and in the interaction space. This analysis also

delivers the amplitudes of the different Floquet harmonics. Both the equivalent resistance of the side resonators and the amplitude of the synchronous Floquet harmonic contribute to the geometrical factor of the RSM. The anode model is then used to calculate the resonant frequencies and to maximize the geometrical term of the rising sun anode in order to minimize the required cathode current. The individual terms are expressed by the equivalent admittance, the  $Q$ -factor, the time-dependent electric field amplitude, and the current density of the interaction space, so that the power balance relation can be solved for the output power. Prescribing frequency and the dimensions of the interaction space finally allows to maximize output power with respect to the dimensions of the anode structure, which is thus optimized. This analysis finally provides the basis for designing the RSM.

As example, we will search for a secondary emission limited mode with potential for CW operation. Moreover, we will apply de-miniaturization in order to meet the requirements of EDM (Electron Discharge Machining) technology even at frequencies above 100 GHz, which have up to today just been reached by the conventional SHM. (In [24], a SHM for 210 GHz has been described.)

Comparing a RSM with a conventional SHM for equal DC beam voltage and magnetic guiding field, the RSM shows higher output power at the sacrifice of doubling the number of side resonators. This disadvantage becomes more and more important for frequencies beyond 100 GHz as can be concluded from the following estimate: The Hartree Resonance Curve defines the relation between magnetic field and the beam voltage, which is directly proportional to the difference between the squared values of anode and cathode diameters. Furthermore, it is inversely proportional to a wave number  $g = |mN/x + n|$  with  $m$  denoting the number of the space harmonic utilized (SHM:  $m = -1$ ),  $N$  means total number of side resonators,  $n$  number of the mode of operation, and  $x$  is a constant (SHM:  $x = 1$ ; RSM:  $x = 2$ ). Mode number  $n$  is an integer with value in between 0 and  $N/x$ . Comparison between RSM and SHM for equal dimensions of cathode and anode (and for the same beam voltage) then yields that the number of side resonators of the RSM is doubled with respect to that of the SHM.



As numerical example, let us choose a frequency of operation of 95 GHz. The optimum anode diameter then is 3.8 mm and the number of side resonators of the SHM is  $N=28$ , leading to an opening width of the side resonators of 0.3 mm. For the RSM then holds  $N=56$  and opening width equal to 0.15 mm. This value is still within the scope of the usual technological tool of EDM. However, at still higher values of the frequency, e.g. at 140 GHz, electric field breakdown in vacuum and the necessity to change the method of fabrication are slowly arising and should influence design and technology. As a consequence, it is desirable – if not even necessary – to find solutions which counteract the problems of miniaturization which arise at increased frequencies. This is of special importance for the RSM with its large number of side resonators. A suitable means for de-miniaturization is enlarging the dimensions in a way that the opening width of the side resonators of the RSM equals that of the SHM.

The number of side resonators of the RSM is twice that of the SHM. If the following parameters of both are kept equal: opening width at the periphery of the interaction space, frequency, mode of operation, and space harmonic, then both the cathode and anode diameters which define the interaction space, must be doubled. Because of the quadratic dependence between beam voltage and both diameters, this means a fourfold increase of that voltage.

To illustrate the situation by an example, let us regard a conventional SHM at frequency of 35 GHz, an anode diameter of 4.5 mm, and a cathode diameter of 2.6 mm. The corresponding relation between beam voltage and magnetic guiding field has been depicted in Fig. 5(a). Stable operation ranges are limited by the regime between the Hartree Resonance Curve and the Hull Cut-Off Parabola. A typical operation point has been denoted by a black square (at a beam voltage of about 11 kV). Next, we will regard an RSM designed for same mode of operation, space harmonic, and frequency but with both the anode and the cathode diameters doubled (which now are 9 and 5.2 mm, respectively). The opening width of the side resonators is still the same, but the necessary beam voltage has to be increased by a factor of 4. This has been illustrated by Fig. 5(b) showing a voltage value of the operation point (square) of almost 45 kV. Such high value will exclude this magnetron oscillator from many technical applications. However, there seems to exist a way out of such dilemma. One could look for an operation point in the lower part of the regime between both limiting curves. An example has been marked in Fig. 5(b) by a red dot. If such operation point at beam voltage of just 6–7 kV and a magnetic field of just 200 kG allows stable operation, an important step toward realization of a sub-THz magnetron has been done.

Another means for de-miniaturization is operating the RSM at a forward harmonic, for instance at the first one. Starting point of a discussion is the formula for the wave number:  $g = |mN/x + n|$  which is evaluated for a SHM with  $m = -1$  and  $n = N/4$  and an RSM with  $m = +1$  and the same  $n = N/4$ . The wave numbers for both devices then are identical:  $g = 3N/4$ . Hence operating the RSM at the first forward harmonic would avoid doubling the number of side resonators. It is hence worth to investigate its features in more detail.

In summary: Both means proposed above – widening the resonance structure and operating at a forward harmonic – show a realistic potential for very low current CW operation. They will probably present a “soft” (with respect to both electrical performance and technological requirements) alternative to the more complex MTM-SHM. Two steps are still to be done: theoretical

investigations and fabrication of prototypes. The tools – the physical description of secs. II and III and EDM technology – are at hand.

## Conclusion

This paper is an extension and a generalization of studies about the meta-material loaded SHM – called MTM-SHM –, which had been published in [25]. A physical design theory is thoroughly derived which – besides showing excellent accuracy w.r.t. simulations with CST Microwave Studio – offers two important advantages: Most of its results are presented by analytical closed-form expressions, and the basic design criterion, for instance maximized output power, appears as product of two factors: one of them just containing geometry and constitutive parameters, the second one just beam current parameters. Hence any design procedure can be based on direct physical insight and on easy and fast evaluations of formulas. Thus the design effort will greatly be reduced in comparison with today’s commercial tools. This feature is demonstrated with several examples taking e.g. mode competition or broadening of the frequency range into account.

Special focus is put on a deep discussion of stability of the oscillations, in particular with respect to lowering the beam current density and thus the thermal loading of the device. Totally different from the conventional SHM (and from the classical magnetron), the MTM-SHM offers stable oscillations with still interesting (probably even superior) margins for output power and efficiency because of the consequences of the product relation described above: Increasing the “geometry factor” for maintaining high output power can be compensated by decreasing the “current factor” appropriately thus re-establishing stability. Moreover, this low-current efficient operation mode is almost independent of frequency so that any upper bound in frequency is exclusively defined by the limits of fabrication technology. The existence of this low-current mode most probably means that a MTM-SHM shows potential for CW operation, a unique feature of this class of magnetrons.

Finally, the investigations are extended to encompass the RSM. It is characterized as “soft alternative” to the MTM-SHM. Instead of MTM loading, it shows twice as many side resonators compared to a conventional SHM. To counteract this feature in order to arrive at almost equal technological requirements for both conventional SHM and RSM, two means are briefly discussed: an RSM employing the first forward spatial harmonic and an RSM with an appropriately widened resonance structure. Interestingly both versions allow low-current and thus CW operation but with reduced output power compared with the MTM-SHM. Hence such a RSM can be regarded as first step toward a MTM-SHM showing similar performance but at a quantitatively reduced level, however, associated with soft requirements to technology.

In summary: A new class of SHMs with the potentials to CW and sub-THz operation has been described, and a physically lucid design theory has been derived. Several interesting and unique features have been outlined. The device is waiting now for deeper investigations.

**Acknowledgements.** The authors gratefully acknowledge Deutsche Forschungsgemeinschaft DFG for financial support.

**Conflict of interest.** None.

## References

- Veselago VG (1968) The electrodynamics of substances with simultaneously negative values of  $\mu$  and  $\epsilon$ . *Soviet Physics Uspekhi* **10**, 509–514.
- Pendry JB, Holden AJ, Robbins DJ and Stewart WJ (1998) Low-frequency plasmons in thin wire structures. *Journal of Physics: Condensed Matter* **10**, 4785–4809.
- Pendry JB, Holden AJ, Robbins DJ and Stewart WJ (1992) Magnetism from conductors and enhanced nonlinear phenomena. *IEEE Transactions on Microwave Theory and Techniques* **MTT-47**, 2075–2081.
- Smith DR, Padilla WJ, Vier DC, Nemat-Nasser SC and Schultz S (2000) Composite medium with simultaneously negative permeability and permittivity. *Physical Review Letters* **84**, 4184–4187.
- Grbic A and Eleftheriades GV (2002) Experimental verification of backward-wave radiation from a negative refractive index metamaterial. *Journal of Applied Physics* **92**, 5930–5935.
- Lu J, Grzegorzczak T, Zhang Y, Pacheco Jr. J, Wu B, Kong J and Chen M (2003) Cherenkov radiation in materials with negative permittivity and permeability. *Optics Express* **11**, 723–734.
- Wu BI, Lu J, Kong JA and Chen M (2007) Left-handed metamaterial design for Čerenkov radiation. *Journal of Applied Physics* **102**, 114907.
- Duan Z, Wu BI, Lu J, Kong JA and Chen M (2008) Cherenkov radiation in anisotropic double-negative metamaterials. *Optics Express* **16**, 18479–18484.
- Xi S, Chen H, Jiang T, Ran L, Huangfu J, Wu BI, Kong JA and Chen M (2009) Experimental verification of reversed Cherenkov radiation in left-handed metamaterial. *Physical Review Letters* **103**, 194801.
- Averkov YO and Yakovenko VM (2005) Cherenkov radiation by an electron bunch that moves in a vacuum above a left-handed material. *Physical Review B* **72**, 205110.
- Konoplev IV, MacLachlan AJ, Robertson CW, Cross AW and Phelps ADR (2011) Cylindrical periodic surface lattice as a metadelectric: concept of a surface-field Cherenkov source of coherent radiation. *Physical Review A* **84**, 013826.
- Genevet P, Wintz D, Ambrosio A, She A, Blanchard R and Capasso F (2015) Controlled steering of Cherenkov surface plasmon wakes with a one-dimensional metamaterial. *Nature Nanotechnology* **10**, 904–905.
- Nasr Esfahani N (2017) Novel spatial harmonic magnetrons and their potential applications. *Proc. 47th Europ. Microwave Conf., Nuremberg*.
- Bliokh YP, Savel'ev S and Nori F (2008) Electron-beam instability in left-handed media. *Physical Review Letters* **100**, 244803.
- Shapiro MA, Trendafilov S, Urzhumov Y, Alu A, Temkin RJ and Shvets G (2012) Active negative-index metamaterial powered by an electron beam. *Physical Review B* **86**, 085132.
- Weiss A and Grbic A (2015) Electron beam coupling to an NRI transmission-line metamaterial. *IEEE Transactions on Plasma Science* **43**, 796–803.
- Tan YS and Seviour R (2009) Wave energy amplification in a metamaterial-based traveling-wave structure. *Europhysics Letters* **87**, 34005.
- Rashidi A and Behdad N (2014) Metamaterial-enhanced traveling wave tubes. *IEEE International Vacuum Electronics Conference (IVEC)*.
- Yan S (1987) The gain calculation of media and electrostatic free electron lasers by Madey theorem. *IEEE Journal of Quantum Electronics* **23**, 1642–1645.
- Nasr Esfahani N, Schuenemann K, Avtomonov N and Vavriv D (2015) Epsilon near zero loaded magnetrons, design and realization. *45th Europ. Microwave Conf., Paris, France*.
- Nasr Esfahani N (2015) Application of metamaterials in spatial harmonic magnetrons. *IEEE Internat. Microwave Symp., Phoenix, USA*.
- Sosnytskiy SV and Vavriv DM (2002) Theory of the spatial-harmonic magnetron: an equivalent network approach. *IEEE Transactions on Plasma Science* **30**, 984.
- Schuenemann K, Serebryannikov AE, Sosnytskiy SV and Vavriv DM (2003) Optimizing the spatial-harmonic millimeter-wave magnetron. *Physics of Plasmas* **7**, 2559–2565.
- Avtomonov NI, Naumenko VD, Vavriv DM, Schuenemann K, Suvorov AN and Markov VA (2012) Towards THz magnetrons: 210 GHz spatial-harmonic magnetron with cold cathode. *IEEE Transactions on Electron Devices* **ED-12**, 3608–3611.
- Nasr Esfahani N (2018) Low-current cathode spatial harmonic magnetrons: analysis and realization based on meta-material loaded slow wave structures. *International Journal of Microwave and Wireless Technologies* **10**, 613–619.
- Collins GB (1948) *Microwave Magnetrons*. New York: Mc-Graw-Hill.
- McDowell HL (2004) Magnetron simulations using a multiple wavelength computer code. *IEEE Transactions on Plasma Science* **PS-32**, 1160–1170.
- Nasr Esfahani N and Schuenemann K (2012) Particle-In-Cell simulation of a spatial-harmonic magnetron with cold secondary-emission cathode. *IEEE Transactions on Plasma Science* **PS-40**, 1512–1519.
- McDowell HL (1998) Magnetron simulations using a moving wavelength computer code. *IEEE Transactions on Plasma Science* **PS-26**, 733–753.

## Appendix

Here is a list of formulas for studying the interdependence between “hot” and “cold” term parts of the electron power.

$$\begin{aligned}
 V_{cold} &= C|\eta_r|\eta_0 d \\
 V_{hot} &= C|\eta_r|\eta_0 da \\
 &= |\eta_r|\eta_0^2 d \frac{A_{-1} X Q_1 C^2 \cos \Delta \varphi}{2 \omega_n} \\
 &= |\eta_r|\eta_0^2 d \frac{A_{-1} X Q_1}{2 \omega_n} \frac{2 \omega_n^2}{N} L \eta_r^{-2} \eta_0^{-2} d^{-2} \cos \Delta \varphi \quad (A.1) \\
 &= \frac{A_{e-1} X Q_1}{2 \omega_n d} \frac{2 \omega_n^2}{N} L \cos \Delta \varphi \\
 &= \frac{A_{-1} X R}{\eta_r d N} \cos \Delta \varphi
 \end{aligned}$$

$$\begin{aligned}
 P_e^U &= \frac{A_{-1}^2 \eta_r^2 \eta_0^2 (\cos \Delta \varphi)^2 X^2 T}{\eta_r^2 2N \sqrt{(\omega_n \mu_0 / 2\sigma)}} = \frac{A_{-1} X R}{\eta_r d N} \cos \Delta \varphi \quad (A.2) \\
 R &= \frac{\mu_z \mu_0 / \epsilon_\varphi \epsilon_0 d^2 \sin^2(k_x l)}{\sqrt{(\omega_n \mu_0 / 2\sigma) H l (1 + (\sin(2k_x l) / 2k_x l) + (d/l))}}
 \end{aligned}$$



**Nasrin Nasr Esfahani** received the B.Sc. (Hons.) and M.Sc. (Hons.) degrees in electrical engineering from Iran University of Science and Technology in Tehran, Iran, in 2004 and 2007 and the Dr.-Ing. degree from Hamburg University of Technology, Germany, in 2014. From 2013 to 2016, she was a scientific assistant at Hamburg University of Technology and at Kiel University. In 2016, she joined the RF group of CERN in Geneva, Switzerland, as a research fellow where she was involved in various RF projects related to the upgrade of the injector chain of the large hadron collider (LHC). Dr. Esfahani's research interests include Terahertz vacuum electronic devices and interaction of beam and waves in these devices, meta-materials (graphene), and theory and design of passive and active microwave components.



**Dmytro D. Vavriv** received Dipl., Ph.D., and D.Sc. degrees from Kharkiv State University in Kharkiv, Ukraine, in 1975, 1979, and 1988, respectively. Since 1989, he is Head of the Department of Microwave Electronics of Institute of Radio Astronomy (National Academy of Sciences of Ukraine) in Kharkiv and a professor at Kharkiv State University. His research activities include millimeter wave

tubes, signal processing, nonlinear phenomena, chaos, remote sensing in meteorology, environmental monitoring, and THz technology.



**Klaus Schünemann** is professor at Hamburg University of Technology, Germany. From 1983 to 2004, he was Director of the Institute of High Frequency Technology. His research interests had been in microwave electronics, field theory, millimeter wave and quasi-optical circuit technologies, and in gyrotron physics and design. Since his retirement in 2004, he is focusing on integrating meta-material structures

in microwave tubes.